Effect of Dispersed MoO_3 Amount on Catalytic Activity of NiO-ZrO_2 Modified with MoO_3 for Acid Catalysis

Jong Rack Sohn,* Sung Gyu Lee, and Dong Cheol Shin

Department of Applied Chemistry, Engineering College, Kyungpook National University, Daegu 702-701, Korea
**E-mail: jrsohn@knu.ac.kr*
Received July 15, 2006

NiO supported on zirconia modified with MoO_3 for acid catalysis was prepared by drying powdered $Ni(OH)_2$-$Zr(OH)_4$ with ammonium heptamolybdate aqueous solution, followed by calcining in air at high temperature. The characterization of prepared catalysts was performed using FTIR, Raman, XRD, and DSC. MoO_3 equal to or less than 15 wt% was dispersed on the surface of catalyst as two-dimensional polymolybdate or monomolybdate, while for MoO_3 above 15 wt%, crystalline orthorhombic phase of MoO_3 was formed, showing that the critical dispersion capacity of MoO_3 on the surface of catalyst is 0.18 g/g NiO-ZrO_2 on the basis of XRD analysis. Acidity and catalytic activities for acid catalysis increased with the amount of dispersed MoO_3. The high acid strength and acidity was responsible for the Mo=O bond nature of the complex formed by the interaction between MoO_3 and ZrO_2. The catalytic activity for acid catalysis was correlated with the acidity of the catalysts measured by the ammonia chemisorption method.

Key Words : NiO-ZrO_2/MoO_3 catalyst, MoO_3 dispersion, Acid catalysis, 2-Propanol dehydration, Cumene dealkylation

Intorduction

Supported metal oxides[1-3] exhibit interesting catalytic behavior depending on the kind of support, the content of active component, and the preparation method. It is well known that the dispersion, the oxidation state, and the structural features of supported species may strongly depend on the support. Structure and physicochemical properties of supported metal oxides are considered to be different compared with bulk metal oxides because of their interaction with supports.

On the other hand, solid acid catalysts play an important role in hydrocarbon conversion reactions in the chemical and petroleum industries.[4,5] Many kinds of solid acids have been found, their acidic properties on catalyst surfaces, their catalytic action, and the structure of acid sites have been elucidated for a long time, and those results have been reviewed by Arata.[6] Zirconium oxide is a very interesting material because of its thermal stability, its mechanical properties and its basic, acidic, reducing, and oxidizing surface properties. Therefore, it is attracting interest in catalysis as a support material as well as a catalyst. The strong acidity of zirconia-supported sulfate has attracted much attention because of its ability to catalyze many reactions such as cracking, alkylation, and isomerization. The potential for a heterogeneous catalyst has yielded many papers on the catalytic activity of sulfated zirconia materials.[6-8] However, catalytic functions have been improved by loading additional components. Sulfated zirconia incorporating Fe and Mn has been shown to be highly active for butane isomerization, catalyzing the reaction even at room temperature.[9,10] Coelho *et al.*[11] have discovered that the addition of Ni to sulfated zirconia causes an activity enhancement comparable to that caused by the addition of Fe and Mn. It has been reported by several workers that the addition of platinum to zirconia modified by sulfate ions enhances the catalytic activity in the skeletal isomerization of alkanes without deactivation when the reaction is carried out in the presence of hydrogen.[12,13] Recently, it has been found that a main group element Al can also promote the catalytic activity and stability of sulfated zirconia in ethylene dimerization and *n*-butane isomerization.[14-16]

Recently, some workers reported zirconia-supported tungsten oxide or molybdenum oxide as alternative materials in reactions requiring strong acid sites.[6,17-19] Several advantages of tungstate or molybdate, over sulfate, as dopant include the facts that it does not suffer from dopant loss during thermal treatment and that it undergoes significantly less deactivation during catalytic reaction.[17] In this paper, these authors tried to prepare other catalyst systems by combining nickel hydroxide to give nickel oxide after decomposition at high temperatures with ZrO_2 modified by MoO_3 which is known to be an acid,[19,20] to improve the catalytic activity for acid catalysis. Especially, the effect of dispersed MoO_3 amount on catalytic activity for acid catalysis was emphasized. For the acid catalysis, the 2-propanol dehydration and cumene dealkylation were used as test reactions.

Experimental Section

Catalyst Preparation. The coprecipitate of $Ni(OH)_2$-$Zr(OH)_4$ was obtained by adding aqueous ammonia slowly into a mixed aqueous solution of nickel chloride and zirconium oxychloride at room temperature with stirring until the pH of mother liquor reached about 8. The coprecipitate thus obtained was washed thoroughly with distilled

water until chloride ion was not detected, and then was dried at 100 °C for 12 h. The dried coprecipitate was powdered below 100 mesh.

The catalysts containing various molybdenum oxide contents were prepared by adding an aqueous solution of ammonium heptamolybdate[$(NH_4)_6(Mo_7O_{24})\cdot 4H_2O$] to the $Ni(OH)_2$-$Zr(OH)_4$ powder, followed by drying and calcining at high temperatures for 1.5 h in air. This series of catalysts are denoted by their weight percentage of NiO and MoO_3. For example, 10-NiO-ZrO_2/15-MoO_3 indicates the catalyst containing 10 wt % NiO regarding only two components, NiO and ZrO_2, and containing 15 wt % MoO_3 regarding all three components, NiO, ZrO_2 and MoO_3.

Procedure. 2-Propanol dehydration was carried out at 160 and 180 °C in a pulse micro-reactor connected to a gas chromatograph. Fresh catalyst in the reactor made of 1/4 in. stainless steel was pretreated at 400 °C for 1 h in a nitrogen atmosphere. Diethyleneglycol succinate on Shimalite was used as packing material of the gas chromatograph and the column temperature for analyzing the product was 150 °C. Catalytic activity for 2-propanol dehydration was represented as mol of propylene converted from 2-propanol per gram of catalyst. Cumene dealkylation was carried out at 400 and 450 °C in the same reactor as above. Packing material for the gas chromatograph was Bentone 34 on Chromosorb W and column temperature was 130 °C. Catalytic activity for cumene dealkylation was represented as mol of benzene converted from cumene per gram of catalyst. The average of the first to sixth pulse values were taken as the conversions for both reactions.

FTIR spectra were obtained in a heatable gas cell at room temperature using a Mattson Model GL6030E spectrophometer. The self-supporting catalyst wafers contained about 9 $mg\cdot cm^{-2}$. Prior to obtaining the spectra we heated the samples under vacuum at 500 °C for 1.5 h.

The Raman spectra were recorded on a Spex Ramalog spectrometer with holographic gratings. The 5145-Å line from a Spectra-Physics Model 165 argon-ion laser was used as the exciting source. The spectral shift width was typically 4 cm^{-1}, and laser source powers of approximately 45 mW, measured at the sample, were used.

Catalysts were checked in order to determine the structure of the support as well as that of molybdenum oxide by means of a Jeol Model JDX-8030 diffractometer, employing Cu Kα (Ni-filtered) radiation.

DSC measurements were performed by a PL-STA model 1500H apparatus in air, and the heating rate was 5 °C per minute. For each experiment, 10-15 mg of sample was used.

The specific surface area was determined by applying the BET method to the adsorption of N_2 at −196 °C. Chemisorption of ammonia was also employed as a measure of the acidity of each catalyst. The amount of chemisorption was determined based on the irreversible adsorption of ammonia.[21-23]

Results and Discussion

Crystalline Structures of Catalysts. The crystalline structures of ZrO_2 and NiO-ZrO_2/MoO_3 calcined in air at different temperatures for 1.5 h were examined. For pure ZrO_2, ZrO_2 was amorphous to X-ray diffraction up to 300 °C, with a two-phase mixture of the tetragonal and monoclinic forms at 400-700 °C and a monoclinic form at 800 °C (This figure is not shown here). Three crystal structures of ZrO_2, tetragonal, monoclinic and cubic phases have been reported.[24,25] However, in the case of NiO-ZrO_2 modified with MoO_3, the crystalline structures of the samples were different from that of pure ZrO_2. For the 10-NiO-ZrO_2/15-MoO_3, as shown in Figure 1, ZrO_2 was amorphous to X-ray diffraction up to 500 °C with tetragonal ZrO_2 form at 600-800 °C. The transition temperature of ZrO_2 from amorphous to tetragonal phase was higher by 200 °C than of pure ZrO_2. However, the higher the calcination temperature, the larger the amount of tetragonal phase of ZrO_2. It is assumed that the interaction between molybdenum oxide (or NiO) and ZrO_2 hinders the transition of ZrO_2 from amorphous to tetragonal phase.[26,27] The presence of molybdenum oxide strongly influences the development of textural properties with temperature. No phase of molybdenum oxide or nickel oxide was observed at any calcination temperature, indicat-

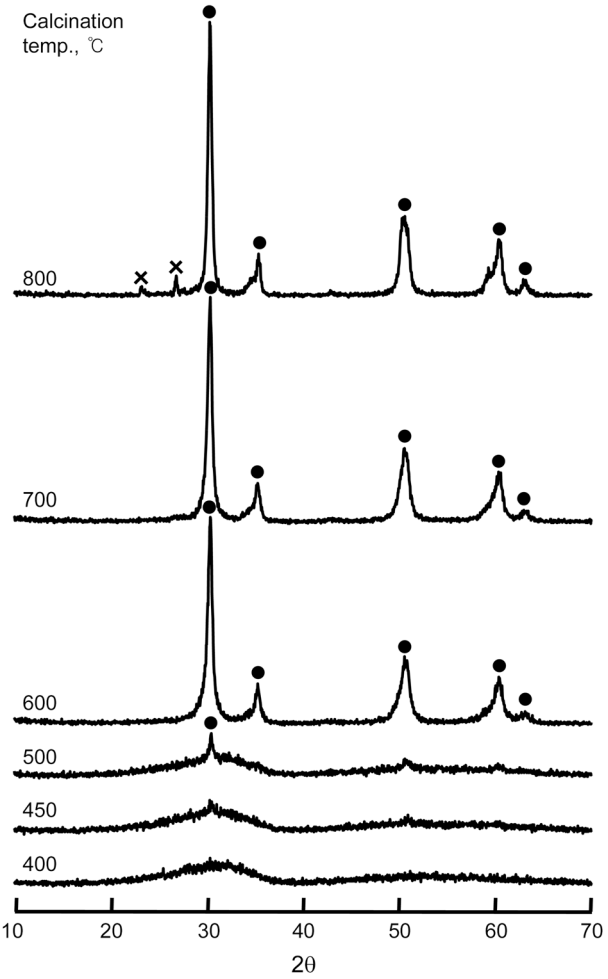

Figure 1. X-ray diffraction patterns of 10-NiO-ZrO_2/15-MoO_3 calcined at different temperatures for 1.5 h: ● , tetragonal ZrO_2; ×, orthorhombic MoO_3.

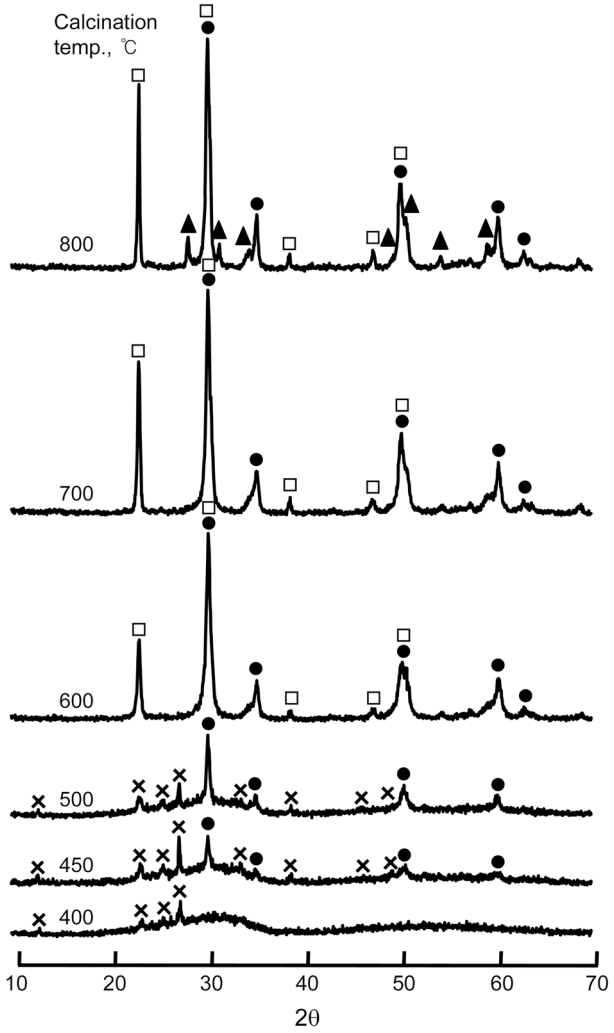

Figure 2. X-ray diffraction patterns of 10-NiO-ZrO_2/25-MoO_3 calcined at different temperatures for 1.5 h: ●, tetragonal ZrO_2; ▲, monoclinic ZrO_2; ×, orthorhombic MoO_3; □, hexagonal $Mo(ZrO_4)_2$.

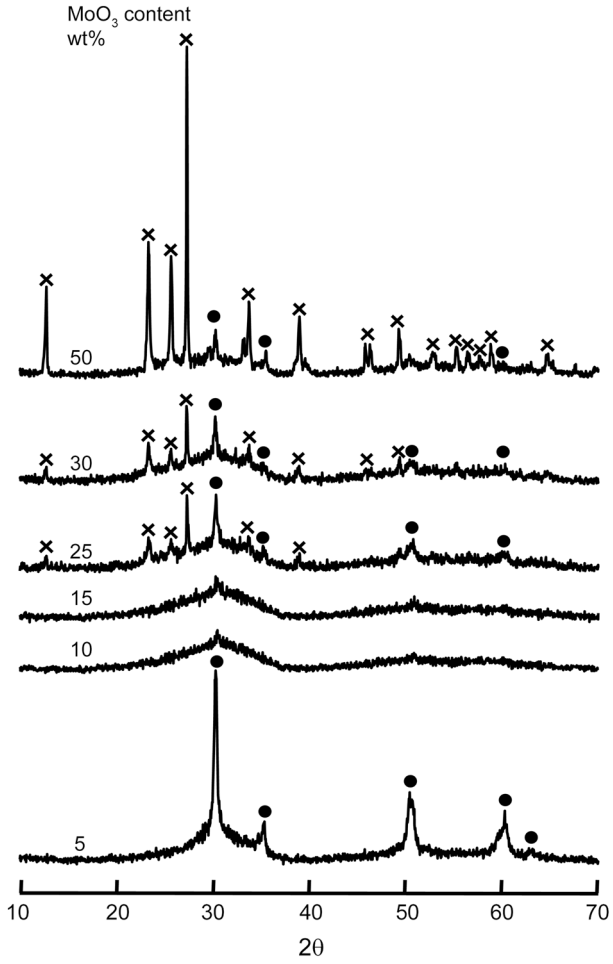

Figure 3. X-ray diffraction patterns of 10-NiO-ZrO_2/MoO_3 containing different MoO_3 contents and calcined at 450 °C for 1.5 h: ●, tetragonal ZrO_2; ×, orthorhombic MoO_3.

ing a good dispersion of molybdenum oxide or nickel oxide on the surface of ZrO_2 support due to the interaction between them.

XRD patterns of 10-NiO-ZrO_2/25-MoO_3 calcined at 400-800 °C for 1.5 h are shown in Figure 2. X-ray diffraction data indicated the amorphous phase of ZrO_2 at 400 °C, showing the tetragonal phase of ZrO_2 at 450-800 °C. However, the higher the calcined temperature, the larger the amount of tetragonal phase of ZrO_2. Moreover, as shown in Figure 2, the orthorhombic phase of MoO_3 was observed at 400-500 °C. It has been reported that MoO_3 for samples containing low MoO_3 loading is dispersed on the surface of zirconia as a monolayer state,[28,29] that is, two-dimensional polymolybdate or monomolybdate, which gives rise to the characteristic broad band at 900-1000 cm^{-1}. However, when MoO_3 loading exceeds a monolayer capacity on the surface of NiO-ZrO_2, the residual crystalline phase of MoO_3 can be detected by XRD, Raman, and IR. From the calcination temperature of 600 °C, a new species, ie., $Zr(MoO_4)_2$ hexagonal phase, has been detected in the 10-NiO-ZrO_2/25-MoO_3 catalyst. As shown in Figure 2, the amount of $Zr(MoO_4)_2$ phase increased with the calcination temperature. Chen *et al.*[30] reported the formation of $Zr(MoO_4)_2$ from MoO_3 and ZrO_2 in high MoO_3 loading sample calcined above 600 °C.

The XRD patterns of 10-NiO-ZrO_2/MoO_3 containing different MoO_3 contents and calcined at 450 °C for 1.5 h are shown in Figure 3. XRD data indicated only tetragonal phase of ZrO_2 at 5 wt% of MoO_3. However, 10-NiO-ZrO_2/10-MoO_3 and 10-NiO-ZrO_2/15-MoO_3 were amorphous to X-ray diffraction, indicating that the increase of MoO_3 loading hinders the phase transition of ZrO_2 from amorphous to tetragonal due to the interaction between MoO_3 and ZrO_2.[16,27] In this case, no detection of orthorhombic phase of MoO_3 means that all MoO_3 is highly dispersed on the surface of NiO-ZrO_2 as two-dimensional polymolybdate or monomolybdate. For the samples containing higher MoO_3 loading than 15 wt%, as shown in Figure 3, the orthorhombic phase of MoO_3 was observed because MoO_3 loading exceeds a monolayer capacity on the surface of ZrO_2, showing that its intensity increases with the MoO_3 content.

When the loading amounts of MoO_3 are low, the highly dispersed molybdenum oxide species can not be detected by

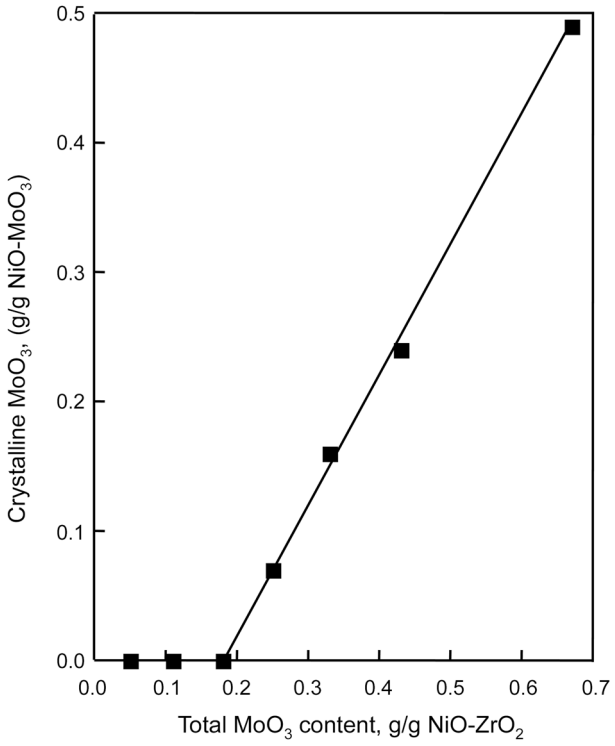

Figure 4. Amount of crystalline MoO_3 against total amount of MoO_3 in 10-NiO-ZrO_2/MoO_3 catalysts containing different MoO_3 contents and calcined at 450 °C for 1.5 h.

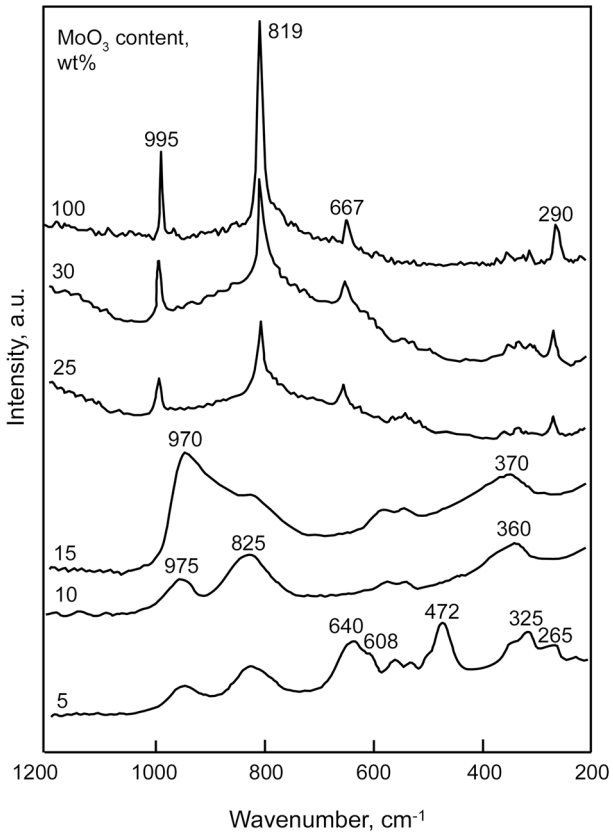

Figure 5. Raman spectra of 10-NiO-ZrO_2/MoO_3 containing different MoO_3 contents and calcined at 450 °C.

XRD, as shown in Figure 3. Therefore, we can estimate the amount of crystalline MoO_3 by the quantitative XRD analysis. Thus, as shown in Figure 4, we can plot the content of crystalline MoO_3 as a function of the total content of MoO_3 in the 10-NiO-ZrO_2/MoO_3 samples containing different MoO_3 contents and calcined at 450 °C, from which the MoO_3 critical dispersion capacity on NiO-ZrO_2, 0.18 g MoO_3/g NiO-ZrO_2 is deduced. Since the surface area of 10-NiO-ZrO_2/15-MoO_3 is 154 m^2/g, this capacity is equivalent to 0.12 g MoO_3/100 m^2 NiO-ZrO_2, which is very similar with the monolayer capacity for MoO_3 supported on ZrO_2.[29] It is expected that this dispersion capacity is related to the surface area and acidity of catalysts as discussed below.

Raman and Infrared Spectra. Raman spectroscopy is a valuable tool for the characterization of dispersed metal oxides and detects vibrational modes of surface and bulk structures. The Raman spectra of MoO_3 obtained by calcining ammonium heptamolybdate at 450 °C and 10-NiO-ZrO_2/MoO_3 containing different MoO_3 contents under ambient conditions are presented in Figure 5. The MoO_3 structure is made up of distorted MoO_3 octahedra. Bulk crystalline MoO_3 shows the main bands, in good agreement with data previously reported[31] and with data of XRD in Figure 2. The major vibrational modes of MoO_3[31] are located at 995, 819, 667, and 290 cm^{-1}, and have been assigned to the Mo=O stretching mode, the Mo-O-Mo stretching mode, OMo_3 vibration mode, and the Mo=O deformation mode, respectively.

The molecular structure of the supported molybdenum oxide species depends on the loading. Several authors observed that the nature of surface molybdenum species on SiO_2, Al_2O_3, TiO_2 and ZrO_2 depends on the amount of MoO_3. A band at about 825 cm^{-1}, corresponding to Mo-O-Mo vibrations,[28,32] and a band at 910-980 cm^{-1}, assigned to Mo=O vibrations in two-dimensional polymolybdate, were observed in these samples.[28,32] Raman bands between 910 and 980 cm^{-1} are usually attributed to the Mo=O vibration of Mo species in either octahedral or tetrahedral environment.[33] Generally, monomolybdate or tetrahedral molybdenum oxygen species have been assigned for low MoO_3 loading samples,[28,33,34] and two-dimensional polymolybdate or octahedral molybdenum-oxygen species with characteristic band around 950-980 cm^{-1}, for high MoO_3 loading samples.[28,33,34] Therefore, the broad band observed in the 900-1000 cm^{-1} region in Figure 5 will be interpreted as an overlap of two characteristic bands for two molybdenum oxide species. The bands around 350-370 cm^{-1} for 10-NiO-ZrO_2/15-MoO_3 and 10-NiO-ZrO_2/10-MoO_3 samples are assigned to Mo=O bending mode.[35]

For 10-NiO-ZrO_2/10-MoO_3 and 10-NiO-ZrO_2/15-MoO_3 in Figure 5, most of zirconia is amorphous to X-ray diffraction, showing tiny amount of tetragonal phase zirconia for the other. The Raman spectrum of amorphous zirconia[36] is characterized by a very weak and broad band at 550-600 cm^{-1}. Tetragonal zirconia[37,38] is expected to yield a spectrum consisting of Raman bands with frequencies at about 148,

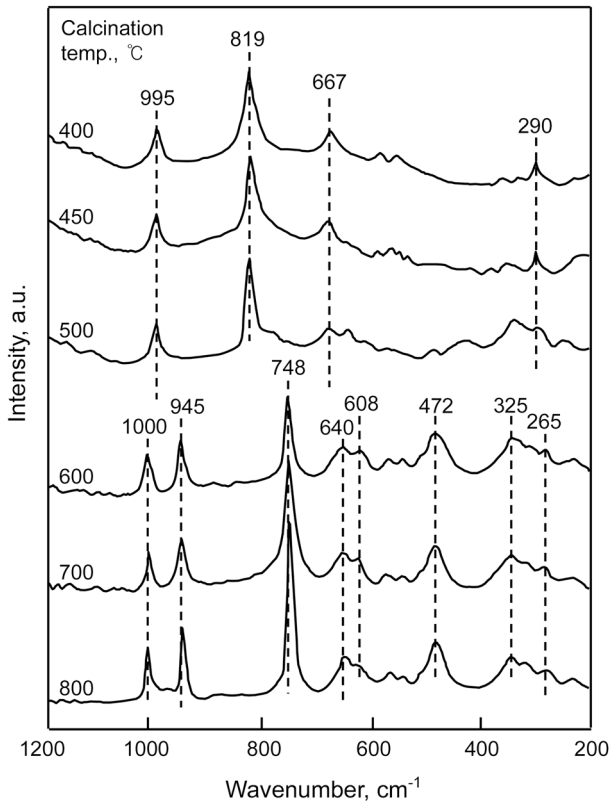

Figure 6. Raman spectra of 10-NiO-ZrO_2/25-MoO_3 calcined at different temperatures for 1.5 h.

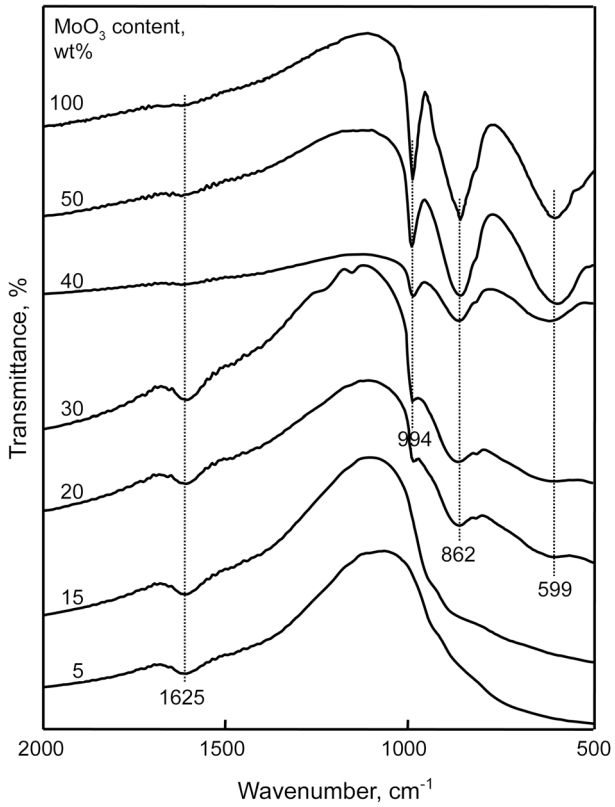

Figure 7. Infrared spectra of 10-NiO-ZrO_2/MoO_3 containing different MoO_3 contents and calcined at 450 °C for 1.5 h.

263, 325, 472, 608, and 640 cm^{-1}, while monoclinic zirconia[37,38] exhibits the characteristic features at 180, 188, 221, 380, 476, and 637 cm^{-1}. As shown in Figure 5, the 10-NiO-ZrO_2/5-MoO_3 sample exhibits the characteristic features of tetragonal zirconia, indicating no transformation of ZrO_2 from tetragonal to monoclinic.

Figure 6 shows Raman spectra of 10-NiO-ZrO_2/25-MoO_3 samples calcined at 400-800 °C for 1.5 h. For sample calcined at 400-500 °C, the vibrational modes of bulk MoO_3 were observed at 995, 819, 667 and 290 cm^{-1} similarly to those of Figure 5. All samples calcined at 450-800 °C except 400 °C also exhibit the characteristic features of tetragonal zirconia at 265, 325, 472, 608, and 640 cm^{-1}, in good agreement with XRD data described above. However, from calcination temperature of 600 °C, a new species, *i.e.*, $Zr(MoO_4)_2$ phase, identified by its characteristic Raman bands[28] at 748, 945, and 1000 cm^{-1}, has been detected in the 10-NiO-ZrO_2/25-MoO_3 catalyst. As shown in Figure 6, the amount of $Zr(MoO_4)_2$ phase increased with the calcination temperature. Chen *et al.*[30] reported the formation of $Zr(MoO_4)_2$ from MoO_3 and ZrO_2 in high loading sample calcined above 600 °C.

Figure 7 shows IR spectra of 10-NiO-ZrO_2/MoO_3 catalysts (KBr disc) with different MoO_3 contents calcined at 450 °C for 1.5 h. Although with samples having less than 20 wt% of MoO_3 no definite peaks were observed, the absorption bands at 994, 862, and 599 cm^{-1} appeared for 10-NiO-ZrO_2/MoO_3 having more than 15 wt% of MoO_3. These bands are due to the crystalline MoO_3. When MoO_3 loading exceeds a certain value, the surplus MoO_3 is present as crystalline form.[28,29,39] In view of Raman spectra of crystalline MoO_3 in Figure 5, for crystalline MoO_3 the IR bands at 991, 870, and 596 cm^{-1} in Figure 7 are assigned to the Mo=O stretching mode, the Mo-O-Mo stretching mode, and OMo_3 vibration mode, respectively. XRD measurements have also supported the presence of the above crystalline MoO_3, as discussed above.

The Raman and IR spectra in Figures 5-7 have been taken in air using the pure powders. To examine the structure of NiO-ZrO_2 modified with MoO_3 under dehydration conditions, IR spectra of 10-NiO-ZrO_2/15-MoO_3 sample were obtained in a heatable gas cell after evacuation at 25 and 500 °C for 1.5 h (This figure is not shown here). For 10-NiO-ZrO_2/15-MoO_3 sample, IR band at 997 cm^{-1} after evacuation at 500 °C is due to the Mo=O stretching mode of the molybdenum oxide complex bonded to the ZrO_2 surface.[40] This Mo=O band due to molybdenyl species only appears on evacuated sample, being shifted on wet sample. The broad band at 944 cm^{-1} under ambient condition is assigned to the terminal Mo=O stretching of the hydrated form of the surface molybdenyl species.[40] This can be rationalized by assuming that the adsorption of water causes a strong perturbation of the corresponding molybdenum oxide species, with a consequent strong broadening and shift down of this band. This isolated molybdenum oxides species is stabilized through multiple Mo-O-Zr bonds between each molybdenum oxide species and the zirconia surface.[28,30] Upon dehydration at

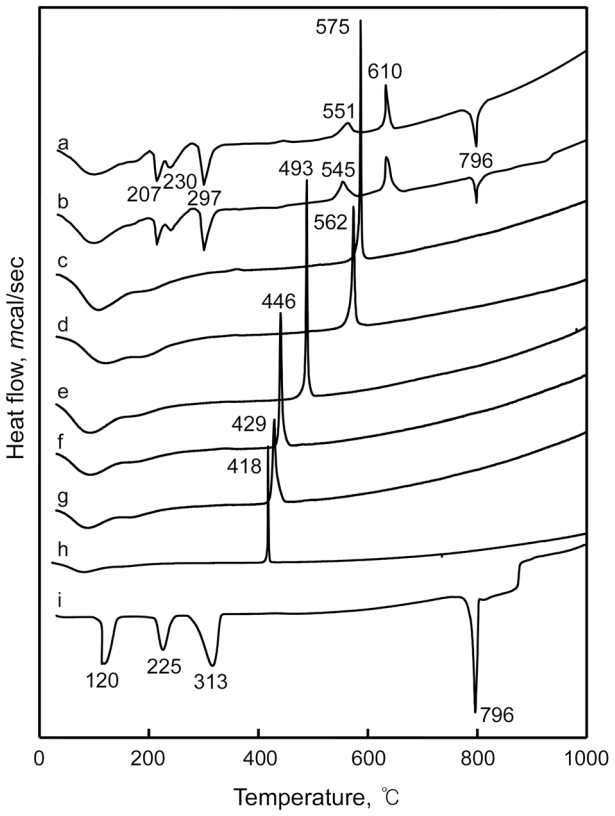

Figure 8. DSC curves of catalyst precursors: (a) 10-NiO-ZrO_2/25-MoO_3, (b) ZrO_2/15-MoO_3, (c) 25-NiO-ZrO_2, (d) 17-NiO-ZrO_2, (e) 10-NiO-ZrO_2, (f) 5-NiO-ZrO_2, (g) 3-NiO-ZrO_2, (h) ZrO_2, and (i) $(NH_4)_6(Mo_7O_{24})\cdot 4H_2O$.

elevated temperature, the hydrated surface metal oxide species is unstable and decompose to form dehydrated surface metal oxide species by direct interaction with the surface OH groups of support, giving the formation of metal-oxygen-support bond.

Thermal Analysis. In X-ray diffraction pattern, it was shown that the structure of NiO-ZrO_2/MoO_3 was different depending on the calcined temperature. To examine the thermal properties for the precusors of samples more clearly, their thermal analysis was carried out and illustrated in Figure 8. For pure ZrO_2 the DSC curve showed a broad endothermic peak below 180 °C due to the elimination of adsorbed water, and an exothermic peak at 418 °C due to the ZrO_2 crystallization.[27,37] For $(NH_4)_6(Mo_7O_{24})\cdot 4H_2O$, the DSC curve shows three endothermic peaks below 400 °C, indicating that the decomposition of ammonium heptamolybdate occurs in three steps. In the case of NiO-ZrO_2/MoO_3, three additional endothermic peaks appeared in the region of 200-400 °C due to the evolution of NH_3 and H_2O decomposed from ammonium heptamolybdate. Also it is considered that an endothermic at 796 °C is responsible for melting of MoO_3[39] and an exothermic peak around 610 °C is due to the formation of $Zr(MoO_4)_2$ described in X-ray diffraction patterns. However, it is of interest to see the influence of NiO and MoO_3 on the crystallization of ZrO_2 from amorphous to tetragonal phase. As Figure 8 shows, the exothermic peak due to the crystallization appears at 418 °C for pure ZrO_2, while for NiO-ZrO_2 and NiO-ZrO_2/MoO_3, it was shifted to higher temperatures. The shift increased with increasing NiO content up to 25 wt% of NiO. It is considered that the interaction between NiO (or MoO_3) and ZrO_2 delays the transition of ZrO_2 from amorphous to tetragonal phase.[16] Consequently, the exothermic peaks appear at 429 °C for 3-NiO-ZrO_2, 446 °C for 5-NiO-ZrO_2, 493 °C for 10-NiO-ZrO_2, 545 °C for ZrO_2/15-MoO_3, 551 °C for 10-NiO-ZrO_2/25-MoO_3, 562 °C for 17-NiO-ZrO_2, and 575 °C for 25-NiO-ZrO_2.

Table 1. Specific surface area and acidity of 10-NiO-ZrO_2/MoO_3 catalysts containing different MoO_3 contents and calcined at 450 °C for 1.5 h

MoO_3 content (wt %)	Surface area (m^2/g)	Acidity (μmol/g)
5	128	112
10	140	134
15	155	141
20	138	129
25	124	121

Table 2. Specific surface area and acidity of NiO-ZrO_2/15-MoO_3 catalysts containing different NiO contents and calcined at 450 °C for 1.5 h

NiO content (wt %)	Surface area (m^2/g)	Acidity (μmol/g)
3	139	78
5	143	119
10	155	141
15	138	137
20	128	121
30	121	95
40	89	78

Surface Properties. It is necessary to examine the effect of molybdenum oxide on the surface properties of catalysts, that is, specific surface area, acidity, and acid strength. The specific surface areas of 10-NiO-ZrO_2/MoO_3 samples calcined at 450 °C for 1.5 h are listed in Table 1. The presence of molybdenum oxide strongly influences the surface area in comparison with the pure ZrO_2. Specific surface areas of 10-NiO-ZrO_2/MoO_3 samples are much larger than that of pure ZrO_2 calcined at the same temperature, showing that surface area increases gradually with increasing molybdenum oxide content up to 15 wt% of MoO_3. The decrease of surface area for samples containing MoO_3 above 15 wt% is due to the blocking of ZrO_2 pore by the increased MoO_3 loading. It seems likely that the interaction between molybdenum oxide and ZrO_2 protects catalysts from sintering. The acidity of catalysts calcined at 450 °C, as determined by the amount of NH_3 irreversibly adsorbed at 230 °C,[16,41,42] is also listed in Table 1. The acidity per surface area for these catalysts was calculated to be nearly constant values of 0.9-1.0 μmol/m^2, indicating that the variation of acidity runs parallel to the change of surface area. We examined the effect of NiO

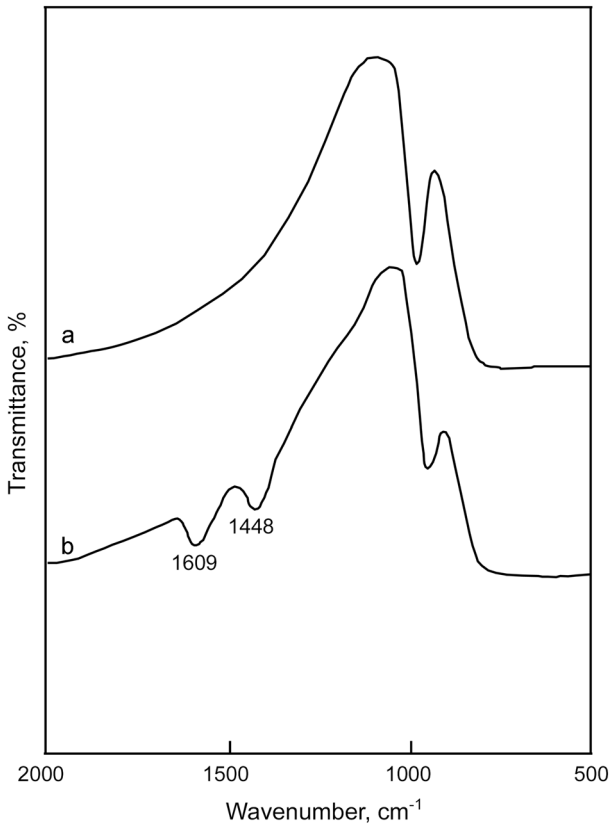

Figure 9. Infrared spectra of NH_3 adsorbed on 10-NiO-ZrO_2/15-MoO_3 : (a) background of 10-NiO-ZrO_2/15-MoO_3 after evacuation at 400 °C for 1 h, (b) NH_3 adsorbed on (a); where gas was evacuated at 230 °C for 1 h.

addition on the surface area and acidity of NiO-ZrO_2/15-MoO_3 catalysts. The specific surface areas and acidity of catalysts calcined at 450 °C are listed in Table 2. Both surface area and acidity increased with increasing NiO content up to 10 wt%, indicating the promoting effect of NiO.

The acid strength of the catalysts was examined by a color change method, using Hammett indicator in sulphurylchloride.[16,19,27] NiO-ZrO_2/MoO_3 was estimated to have a $H_0 \leq -14.5$, indicating the formation of new acid sites stronger than those of single oxide components. Acids stronger than $H_0 \leq -11.93$, which corresponds to the acid strength of 100% H_2SO_4, are superacids.[6,43,44] Consequently, NiO-ZrO_2/MoO_3 catalysts would be solid superacids. The superacidic property is attributed to the double bond nature of the Mo=O in the complex formed by the interaction of ZrO_2 with molybdate, in analogy with the case of ZrO_2 modified with tungstate, chromate, and sulfate ions.[27,45]

Infrared spectroscopic studies of ammonia adsorbed on solid surface have made it possible to distinguish between Brönsted and Lewis acid sites.[16,19,41] Figure 9 shows the IR spectra of ammonia adsorbed on 10-NiO-ZrO_2/15-MoO_3 evacuated at 400 °C for 1 h. The band at 1448 is the characteristic peak of ammonium ion, which is formed on the Brönsted acid sites and the absorption peak at 1609 cm^{-1} is contributed by ammonia coordinately bonded to Lewis acid sites,[16,46,47] indicating the presence of both Brönsted and

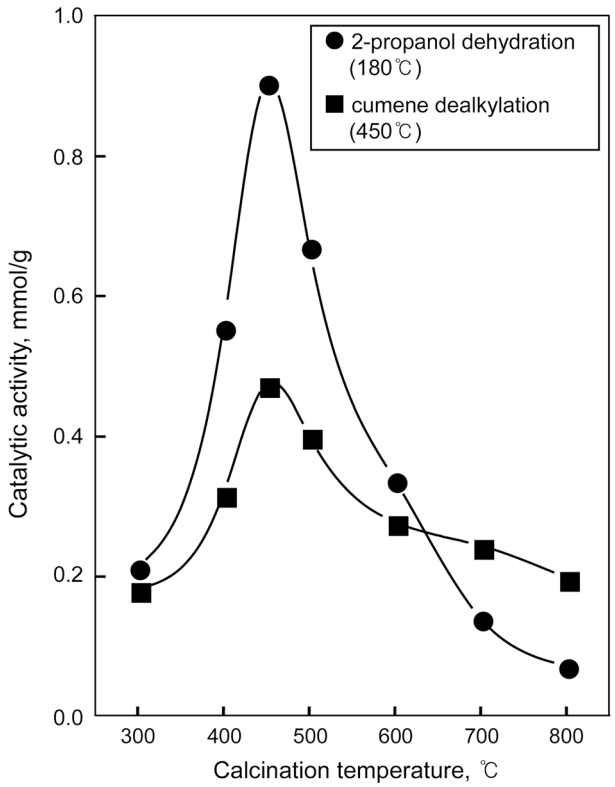

Figure 10. Catalytic activities of 10-NiO-ZrO_2/15-MoO_3 for (●) 2-propanol dehydration and (■) cumene dealkylation as a function of calcination temperature.

Lewis acid sites on the surface of catalyst. Other samples having different MoO_3 contents also showed the presence of both Lewis and Brönsted acid sites.

Catalytic Activities for Acid Catalysis. Catalytic activities of 10-NiO-ZrO_2/15-MoO_3 for 2-propanol dehydration and cumene dealkylation are plotted as a function of calcination temperature in Figure 10, where reaction temperatures are 180 °C for 2-propanol dehydration and 450 °C for cumene dealkylation, respectively. The activities for both reactions increased with the calcination temperature, reaching a maximum at 450 °C, after which the activities decreased. The decrease of activities for both reactions above 450 °C can be attributed to the fact that the surface area and acidity above 450 °C decrease with the calcination temperature. In fact, the surface area and acidity for 10-NiO-ZrO_2/15-MoO_3 calcined at 450 °C were 154 m^2/g and 140 μmol/g, respectively, while those for the catalyst calcined at 800 °C were found to be 45 m^2/g and 58 μmol/g, respectively. Thus, hereafter, emphasis is placed only on the catalysts calcined at 450 °C.

Effect of Dispersed MoO_3 Amount on Acidity and Catalytic Activity. The forms of active components present in heterogeneous catalysts are of importance to catalysis. A great many oxides can disperse spontaneously onto the surface of supports to form a monolayer, because the monolayer is a thermodynamically stable form.[39] Dispersed MoO_3 amount, surface area, acidity, and catalytic activity for 10-NiO-ZrO_2/MoO_3 catalysts containing MoO_3 content below 20 wt% are listed in Table 3. There are good correlations

Table 3. Dispersed MoO_3 amount, specific surface area, acidity, and catalytic activity of 10-NiO-ZrO_2/MoO_3 catalysts containing MoO_3 content below 20 wt%

Catalyst	Dispersed MoO_3 amount (MoO_3 g/NiO-ZrO_2 g)	Surface area (m^2/g)	Acidity (μmol/g)	Catalytic activity	
				2-propanol dehydration (mmol/g)	Cumene dealkylation (mmol/g)
10-NiO-ZrO_2/5-MoO_3	0.05	128	112	0.21	0.12
10-NiO-ZrO_2/10-MoO_3	0.11	140	134	0.70	0.24
10-NiO-ZrO_2/15-MoO_3	0.18	154	140	0.92	0.48

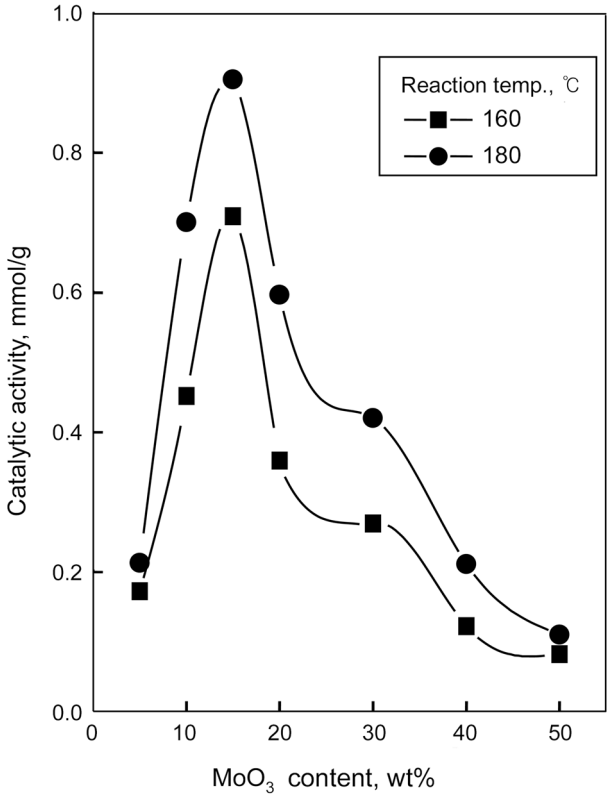

Figure 11. Catalytic activities of 10-NiO-ZrO_2/MoO_3 for 2-propanol dehydration as a function of MoO_3 content.

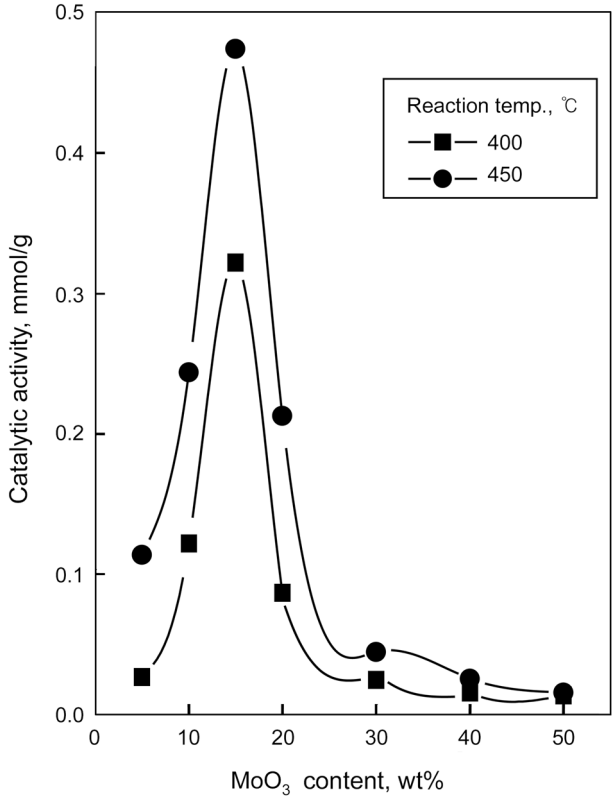

Figure 12. Catalytic activities of 10-NiO-ZrO_2/15-MoO_3 for cumene dealkylation as a function of MoO_3 content.

among the dispersed MoO_3 amount, acidity, and catalytic activity. Namely, the larger the dispersed MoO_3 amount, the higher both acidity and catalytic activity. This can be explained in terms of that strong acid sites are formed through the bonding between dispersed MoO_3 and ZrO_2 and consequently catalytic activity increases due to the increased acid sites.

The catalytic activities for 2-propanol dehydration and cumene dealkylation as a function of MoO_3 content are plotted in Figures 11 and 12, respectively. The maximum activities for both reactions are obtained with the catalyst containing 15 wt% MoO_3, where the amount of dispersed MoO_3 is also maximum. It seems likely that the highest activity of the catalyst containing 15 wt% MoO_3 is related to its acidity and acid strength. The high acid strength and acidity are responsible for the Mo=O bond nature of complex formed by the interaction between MoO_3 and ZrO_2.[6,19] As discussed in IR spectra, IR spectra of 10-NiO-ZrO_2/15-MoO_3 sample after evacuation at 500 °C showed the band at 997 cm^{-1} due to the Mo=O stretching mode of the molybdenum oxide complex bonded to the ZrO_2 surface.[40] This isolated molybdenum oxide species is stabilized through multiple Mo-O-Zr bonds between each molybdenum oxide species and the zirconia surface.[28,30] As listed in Tables 1 and 3, the acidity of 10-NiO-ZrO_2/15-MoO_3 is the most among the catalysts. Of course, the acidity of catalysts is related to their specific surface area, as mentioned above. In fact, Tables 1 and 3 show that the specific surface area attained a maximum when the MoO_3 content in 10-NiO-ZrO_2/MoO_3 is 15 wt%. Although the sample without MoO_3 was inactive as acid catalyst, as shown in Figures 11 and 12, the 10-NiO-ZrO_2/MoO_3 with MoO_3 exhibited high catalytic activity for acid catalysis.

Correlation between Catalytic Activity and Acidity. It is interesting to examine how the catalytic activity of acid catalyst depends on the acid property. For both 2-propanol

dehydration and cumene dealkylation reactions NiO-ZrO_2/MoO_3 catalysts calcined at 450 °C exhibited the highest catalytic activities. In view of Table 1 and Figure 11, the variation in catalytic activity for 2-propanol dehydration is correlated with the change of their acidity, showing the highest activity and acidity for 10-NiO-ZrO_2/15-MoO_3. It has been known that 2-propanol dehydration takes place very readily on weak acid sites.[21,48] Good correlations have been found in many cases between the acidity and the catalytic activities of solid acids. For example, the rates of both the catalytic decomposition of cumene and the polymerization of propylene over SiO_2-Al_2O_3 catalysts were found to increase with increasing acid amounts at strength $H_0 \leq +3.3$.[49] The catalytic activities for both reactions, 2-propanol dehydration and cumene dealkylation, were correlated with the acidity of $NiSO_4$ supported on TiO_2-ZrO_2 measured by an ammonia chemisorption method. It was also reported that the catalytic activity of nickel silicates in the ethylene dimerization as well as in the butene isomerization was closely correlated with the acid amount of the catalyst.[50,51]

Cumene dealkylation takes place on relatively strong acid sites of the catalysts.[21,48] Catalytic activity for cumene dealkylation against MoO_3 content is presented in Figure 12, where reaction temperature is 400-450 °C. Comparing Table 1 and Figure 12, the catalytic activity is also correlated with the acidity. The correlation between catalytic activity and acidity holds for both reactions, cumene dealkylation and 2-propanol dehydration, although the acid strength required to catalyze acid reaction is different depending on the type of reactions.[21,48] As seen in Figures 11 and 12, the catalytic activity for cumene dealkylation, in spite of higher reaction temperature, is lower than that for 2-propanol dehydration.

The acidity of the catalysts can be also correlated to the amount of dispersed MoO_3. As listed in Table 3, the maximum acidity is obtained with the catalyst containing 15 wt% MoO_3, where the amount of dispersed MoO_3 is also maximum. The acidity of NiO-ZrO_2/MoO_3 calcined at 450 °C was determined by the amount of NH_3 irreversibly adsorbed at 230 °C.[16,41,42] As listed in Tables 1 and 2, the BET surface area and acidity attained a maximum extent for the 10-NiO-ZrO_2/15-MoO_3 catalyst. However, as mentioned above, 2-propanol dehydration takes place very readily on weak acid sites, while cumene dealkylation takes place on relatively strong acid sites.[21,48] Therefore, it seems likely that the patterns of catalytic activities for both reactions as a function of MoO_3 content are more or less different.

Effect of NiO on Catalytic Activity. To examine the promoting effect of NiO on the catalytic activities, the catalytic activities of NiO-ZrO_2/15-MoO_3 for 2-propanol dehydration and cumene dealkylation are plotted as a function of NiO in Figure 13. For both reactions the catalytic activities increased with increasing NiO content up to 10 wt%, and then decreased. However, in view of Table 2 and Figure 13, the increases of catalytic activities by the addition of NiO seem to be correlated with the acidity of catalysts, because the addition of NiO brought about the increase of acidity as

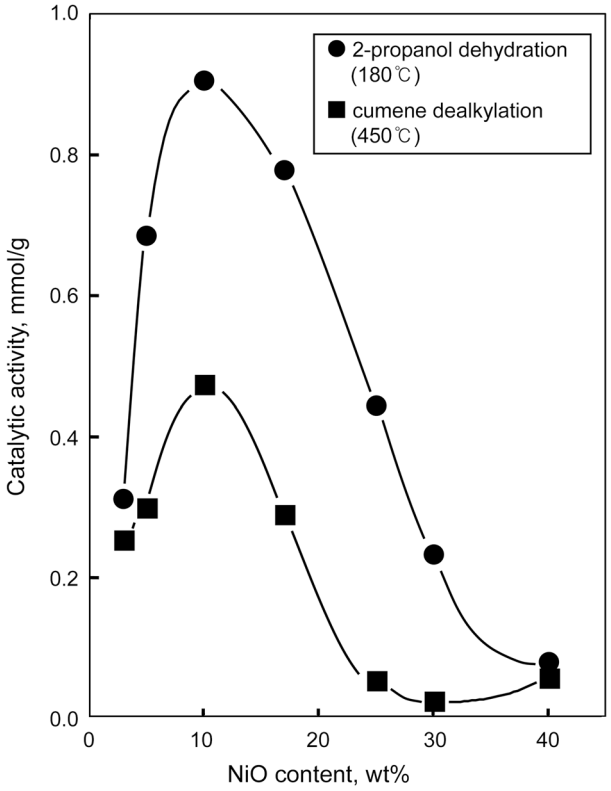

Figure 13. Catalytic activities of NiO-ZrO2/15-MoO_3 for (●) 2-propanol dehydration and (■) cumene dealkylation as a function of NiO content.

listed in Table 2. The presence of NiO may attract reactants and enhance the local concentration of reactants near the acid sites,[52] consequently showing the increased catalytic activities. Conclusively, the addition of NiO (10 wt%) increased not only acidity, but enhanced the concentration of reactants near the acid sites. The high acid strength and high acidity of catalysts modified with MoO_3 are also responsible for the Mo=O bond nature of complex formed by the interaction between dispersed MoO_3 and ZrO_2. Therefore, 10-NiO-ZrO_2/15-MoO_3 exhibited the maximum catalytic activities for acid catalysis.

Conclusions

NiO-ZrO_2/MoO_3 catalysts were prepared by adding an aqueous solution of ammonium metatungstate to the $Ni(OH)_2$-$Zr(OH)_4$ powder, followed by drying and calcining at high temperatures for 1.5 h in air. The interaction between molybdenum oxide (or nickel oxide) and zirconia influences the physicochemical properties of prepared catalysts with calcination temperature. The interaction between MoO_3 (or NiO) and ZrO_2 delayed the phase transition of ZrO_2 from amorphous to tetragonal. Since the ZrO_2 stabilizes the surface molybdenum oxide species, for the samples equal to or less than 15 wt%, molybdenum oxide was well dispersed on the surface of zirconia, but for the samples above 15 wt% the orthorhombic phase of MoO_3 was observed at the calcination temperature of 450 °C. The larger the dispersed

MoO_3 amount, the higher both acidity and catalytic activities for acid catalysis, because strong acid sites are formed through the bonding between dispersed MoO_3 and ZrO_2. The high acid strength and high acidity are responsible for the Mo=O bond nature of complex formed by the interaction between MoO_3 and ZrO_2.

Acknowledgement. We wish to thank Korea Basic Science Institute for the use of Raman and X-ray Instruments.

References

1. Wainwright, M. S.; Foster, N. R. *Catal. Rev.* **1979**, *19*, 211.
2. Dadyburjor, D. B.; Jewur, S. S.; Ruckenstein, E. *Catal. Rev.* **1979**, *19*, 293.
3. Sohn, J. R. *J. Ind. Eng. Chem.* **2004**, *10*, 1.
4. Cheung, T. K.; d'Itri, J. L.; Lange, F. C.; Gates, B. C. *Catal. Lett.* **1995**, *31*, 153.
5. Tanabe, K.; Misono, M.; Ono, Y.; Hattori, H. *New Solid Acids and Bases*; Elsevier Science: Amsterdam, 1989; Chapter 4.
6. Arata, K. *Adv. Catal.* **1990**, *37*, 165.
7. Ward, D. A.; Ko, E. I. *J. Catal.* **1994**, *150*, 18.
8. Kustov, L. M.; Kazansky, V. B.; Figueras, F.; Tichit, D. *J. Catal.* **1994**, *150*, 143.
9. Hsu, C. Y.; Heimbuch, C. R.; Armes, C. T.; Gates, B. C. *J. Chem. Soc., Chem. Commun.* **1992**, 1645.
10. Cheung, T. K.; Gates, B. C. *J. Catal.* **1997**, *168*, 522.
11. Coelho, M. A.; Resasco, D. E.; Sikabwe, E. C.; White, R. L. *Catal. Lett.* **1995**, *32*, 253.
12. Hosoi, T.; Shimadzu, T.; Ito, S.; Baba, S.; Takaoka, H.; Imai, T.; Yokoyama, N. *Prepr. Symp. Div. Petr. Chem.*; American Chemical Society: LosAngels, CA, 1988; p 562.
13. Ebitani, K.; Konishi, J.; Hattori, H. *J. Catal.* **1991**, *130*, 257.
14. Hua, W.; Xia, Y.; Yue, Y.; Gao, Z. *J. Catal.* **2000**, *196*, 104.
15. Moreno, J. A.; Poncelet, G. *J. Catal.* **2001**, *203*, 453.
16. Sohn, J. R.; Cho, E. S. *Appl. Catal. A : Gen.* **2005**, *282*, 147.
17. Larsen, G.; Lotero, E.; Parra, R. D. *In Proceeding of the 11th International Congress on Catalysis*; Elsevier: New York, 1996; pp 543-551.
18. Hino, M.; Arata, K. *J. Chem. Soc., Chem. Commun.* **1987**, 1259.
19. Sohn, J. R.; Chun, E. W.; Pae, Y. I. *Bull. Korean Chem. Soc.* **2003**, *24*, 1785.
20. Brown, A. S. C.; Hargreaves, J. S. J.; Taylor, S. H. *Catal. Letts.* **1999**, *57*, 109.
21. Sohn, J. R.; Lee, S. H. *Appl. Catal. A: Gen.* **2004**, *266*, 89.
22. Sohn, J. R.; Han, J. S. *J. Ind. Eng. Chem.* **2005**, *11*, 439.
23. Sohn, J. R.; Han, J. S.; Kim, H. W.; Pae, Y. I. *Bull. Korean Chem. Soc.* **2005**, *26*, 755.
24. Larsen, G.; Lotero, E.; Petkovic, L. M.; Shobe, D. S. *J. Catal.* **1997**, *169*, 67.
25. Afanasiev, P.; Geantet, C.; Breysse, M.; Coudurier, G.; Vedrine, J. C. *J. Chem. Soc., Faraday Trans.* **1994**, *190*, 193.
26. Sohn, J. R.; Kim, Y. T.; Shin, D. C. *Bull. Korean Chem. Soc.* **2005**, *26*, 1479.
27. Sohn, J. R.; Cho, S. G.; Pae, Y. I.; Hayashi, S. *J. Catal.* **1996**, *159*, 170.
28. Liu, Z.; Chen, Y. *J. Catal.* **1998**, *177*, 314.
29. Zhao, B.; Wang, X.; Ma, H.; Tang, Y. *J. Mol. Catal. A: Chem.* **1996**, *108*, 167.
30. Chen, K.; Xie, S.; Iglesia, E.; Bell, A. T. *J. Catal.* **2000**, *189*, 421.
31. Smith, M. R.; Ozkan, U. S. *J. Catal.* **1993**, *141*, 124.
32. Mestl, G.; Srinivasan, T. K. K. *Cat. Rev. Sci. Eng.* **1998**, *40*, 451.
33. Dufresne, P.; Payen, E.; Grimblot, J.; Bonnelle, J. P. *J. Phys.Chem.* **1981**, *85*, 2344.
34. Hu, H.; Wachs, I. E. *J. Phys. Chem.* **1995**, *99*, 10897.
35. Roark, R. D.; Kohler, S. D.; Ekerdt, J. G.; Kim, D. S.; Wachs, I. E. *Catal. Lett.* **1992**, *16*, 77.
36. Schild, C. H.; Wokaun, A.; Köppel, R. A.; Baiker, A. *J. Catal.* **1991**, *130*, 657.
37. Sohn, J. R.; Doh, I. J.; Pae, Y. I. *Langmuir* **2002**, *18*, 6280.
38. Scheithauer, M.; Grasselli, R. K.; Knözinger, H. *Langmuir* **1998**, *14*, 3019.
39. Xie, Y. C.; Tang, Y. Q. *Adv. Catal.* **1990**, *37*, 1.
40. Litteti, L.; Nova, I.; Ramis, G.; DallAcqua, L.; Busca, G.; Giamello, E.; Forzatti, P.; Bregani, F. *J. Catal.* **1999**, *187*, 419.
41. Sohn, J. R.; Lim, J. S. *Catal. Today* **2006**, *111*, 403.
42. Sohn, J. R.; Han, J. S. *Appl. Catal. A: Gen.* **2006**, *298*, 168.
43. Olah, F. G. A.; Prakash, G. K. S.; Sommer, J. *Science* **1979**, *206*, 13.
44. Tanabe, K.; Misono, M.; Ono, Y.; Hattori, H. *New Solid Acids and Bases*; Elsevier Science: Amsterdam, 1989; p 185.
45. Sohn, J. R.; Ryu, S. G. *Langmuir* **1993**, *9*, 126.
46. Basila, M. R.; Kantner, T. R. *J. Phys. Chem.* **1967**, *71*, 467.
47. Satsuma, A.; Hattori, A.; Mizutani, K.; Furuta, A.; Miyamoto, A.; Hattori T.; Murakami, Y. *J. Phys. Chem.* **1988**, *92*, 6052.
48. Decanio, S. J.; Sohn, J. R.; Fritz, P. O.; Lunsford, J. H. *J. Catal.* **1986**, *101*, 132.
49. Tanabe, K. *Solid Acids and Bases*; Kodansha: Tokyo, 1970; p 103.
50. Sohn, J. R.; Park, W. C. *Appl. Catal. A: General* **2003**, *239*, 269.
51. Sohn, J. R.; Ozaki, A. *J. Catal.* **1980**, *61*, 29.
52. Pae, Y. I.; Bae, M. H.; Park, W. C.; Sohn, J. R. *Bull. Korean Chem. Soc.* **2004**, *25*, 1881.